

# Fast ignition of fusion targets by laser-driven electrons

**J.J. Honrubia**

E.T.S.I. Aeronáuticos, Universidad Politécnica de Madrid, Spain

E-mail: javier.honrubia@upm.es

**J. Meyer-ter-Vehn**

Max-Planck-Institut für Quantenoptik, Garching, Germany

**Abstract.** We present hybrid PIC simulations of fast electron transport and energy deposition in pre-compressed fusion targets, taking full account of collective magnetic effects and the hydrodynamic response of the background plasma. Results on actual ignition of an imploded fast ignition configuration are shown accounting for the increased beam divergence found in recent experiments [J.S. Green et al., Phys. Rev. Lett. **100**, 015003 (2008)] and the reduction of the electron kinetic energy due to profile steepening predicted by advanced PIC simulations [B. Chrisman et al. Phys. Plasmas **15**, 056309 (2008)]. Target ignition is studied as a function of injected electron energy, distance of cone-tip to dense core, initial divergence and kinetic energy of the relativistic electron beam. We found that beam collimation reduces substantially the ignition energies of the cone-guided fuel configuration assumed here.

## 1. Introduction

Fast ignition [1, 2] involves transport of GA currents of laser-driven electrons through dense coronal plasma of imploded fusion targets. Recent studies [3, 4] have shown that the beam can undergo the resistive filamentation instability when passing through coronal plasma and that beam collimation by self-generated fields can reduce ignition energies substantially. These results were obtained for rather focused beams (initial divergence half-angle =  $22^\circ$ ) with electron kinetic energies given by the ponderomotive scaling. Recent experiments [5, 6] have evidenced an increase of beam divergence with laser intensity, e.g. electron effective propagation angles of  $35^\circ$  have been reported for fast ignition relevant conditions. In addition, advanced PIC simulations [7] have shown that the ponderomotive scaling overestimates fast electron kinetic energies due to the plasma electron density profile steepening caused by photon pressure at laser irradiances of the order of  $10^{20}$  W/cm<sup>2</sup>. In this paper, we broaden the scope of our previous studies [3, 4] and present results on actual ignition of an imploded fast ignition configuration accounting for the increase of the beam divergence and the reduction of the electron kinetic energy mentioned above. In addition, we assume a supergaussian distribution

in radius of the beam electrons to enhance azimuthal magnetic field generation and beam collimation. An imploded cone-guided fuel configuration is considered, and target ignition is studied as a function of injected electron energy, distance of cone-tip to dense core, initial divergence and mean kinetic energy of the relativistic electron beam. The present study has been motivated by the future fast ignition facilities such as HiPER [8].

In the hybrid approach pursued here, the relativistic electron beam is treated by 2D/3D PIC including collisional energy loss, while the high density background plasma is modelled by resistive MHD equations including hydrodynamic motion to describe magnetic field suppression by plasma return currents. Full scale kinetic simulation may become possible in the future [7], but presently the hybrid approach pursued here offers a unique option to investigate important transport features such as current filamentation and magnetic beam collimation simultaneously with ignition physics (fusion reactions,  $\alpha$ -particle transport and deposition, thermal radiation transport, hydrodynamics and heat conduction). One may recall that, so far, most fast ignition simulations [9] assumed ballistic straight-line beam transport, neglecting all the intricacies of high-current (GA) transport in plasma.

The present paper is organised as follows. In Section 2, the simulation model and the initial distribution function assumed for the fast electron beam are described. In Section 3, the imploded fuel target configuration and the beam parameters used in our study are presented. In Section 4, we analyse the fast electron energy deposition in the target. In Sections 5 and 6, the coupling efficiencies and the ignition energies are parametrically studied, respectively, as a function of cone-tip to dense core distance, initial divergence and mean kinetic energy of the fast electron beam. Finally, in Section 6 we summarise our results.

## 2. Simulation model

We used the hybrid model proposed by Bell [10] and further developed by Davies [11] and Gremillet et al. [12]. This model is adequate for describing self-magnetized transport in high-density fuel, where kinetic energy transfers and most of the beam-plasma instabilities are suppressed by collisions. It treats only the relativistic beam electrons by PIC and models the background plasma by the return current density  $\mathbf{j}_r$ , tied to the electric field  $\mathbf{E}$  by Ohm's law with resistivity  $\eta$ . Maxwell's equations are used in the form

$$\mathbf{E} = \eta \mathbf{j}_r, \quad (1)$$

$$\mathbf{j}_b + \mathbf{j}_r = \frac{1}{\mu_0} \nabla \times \mathbf{B}, \quad (2)$$

$$\partial \mathbf{B} / \partial t = -\nabla \times \mathbf{E}, \quad (3)$$

where  $\mathbf{j} = \mathbf{j}_b + \mathbf{j}_r$  is the net current density, defined as the sum of beam and return current densities. The displacement current and charge separation effects can be neglected since in this high-density environment relaxation times and Debye lengths are much smaller

than the sub-picosecond and micrometer scales in which we are interested here. The recent study by Kemp et al. [13] justifies to choose resolution less than the Debye and skin lengths at high densities due to the suppression of collective effects by collisions. In the present model, the beam deposits energy into plasma electrons by direct classical Coulomb deposition and via return current Ohmic heating with power density  $\eta j_r^2$ . Our hybrid-PIC approach reproduces cone-target experiments [14, 15], similar to previous hybrid simulations [16, 17]. Since laser pulses of about 15 ps are needed to ignite the pre-compressed fuel, we have included in our model thermal electron conduction, multigroup radiation transport, fusion reactions, alpha particle transport and energy deposition, and hydrodynamics. This integrated model is used here in 2D r - z cylindrical geometry mode. It is worth pointing out that previous hybrid simulations [3, 16, 17] assumed a stationary background plasma while in the present model plasma motion is described by radiation-hydrodynamic equations. The details of the fast electron transport code can be found in [18, 19, 20].

We assume in the present calculations that beam filamentation at the cone tip [17, 21] or Weibel and two-stream instabilities [22, 23] in the low density zones do not perturb beam propagation from the critical surface to the minimum density of  $2 \text{ g/cm}^3$  considered in this paper. This is supported by the cone target experiments carried out by Kodama et al. [14, 15] and also by the recent PIC calculations by Chrisman, Sentoku and Kemp [7] showing that, even though the fast electron beam is split into filaments at the cone tip, these filaments are strongly damped in the dense plasma beyond the cone.

Because the ultra-intense laser pulse interaction with the cone cannot be described by hybrid codes, we rather model the injected beam in form of a directed energy distribution typically fitted to PIC simulations [7, 24] or experiments [14, 15, 25]. The energy distribution of beam electrons is assumed to be one-dimensional (1D) relativistic Maxwellian with temperature  $kT_b = f_T \times m_e c^2 [(1 + I\lambda^2/1.37 \times 10^{18})^{1/2} - 1]$  obtained for local laser intensity  $I$  (in units of  $\text{W/cm}^2$ ) and wavelength  $\lambda$  (in  $\mu\text{m}$ ). Here,  $f_T$  is a parameter that accounts for the plasma electron density profile steepening due to the laser ponderomotive force reported in Ref. [7]. We assume  $f_T = 0.80, 0.67$  and  $0.51$  to obtain electron mean kinetic energies of 2.0, 1.6 and 1.2 MeV for a laser intensity of  $2 \times 10^{20} \text{ W/cm}^2$  and  $\lambda = 0.53 \mu\text{m}$ , respectively $\ddagger$ . We have chosen the 1D relativistic Maxwellian distribution due to the 1D character of the electron acceleration by ultra-intense laser pulses. In addition, the lack of experimental data about spectra of electron beams produced by laser pulses of a few times  $10^{20} \text{ W/cm}^2$  and 10 - 20 ps duration also supports our choice. It is worthwhile pointing out that the mean energy of the 1D relativistic Maxwellian distribution ( $\langle E \rangle_{1D} = kT$  in the ultra-relativistic limit) is substantially lower than that corresponding to the 3D relativistic Maxwellian one ( $\langle E \rangle_{3D} = 3kT$  in the ultra-relativistic limit) for the same laser intensity, leading to beam electrons with lower kinetic energy and penetration depth.

$\ddagger$  For electron temperatures  $kT_b = 2.24, 1.88$  and  $1.43 \text{ MeV}$ , the 1D relativistic Maxwellian distribution gives  $\langle E \rangle/kT_b \approx 0.88, 0.86$  and  $0.84$ , respectively.

!

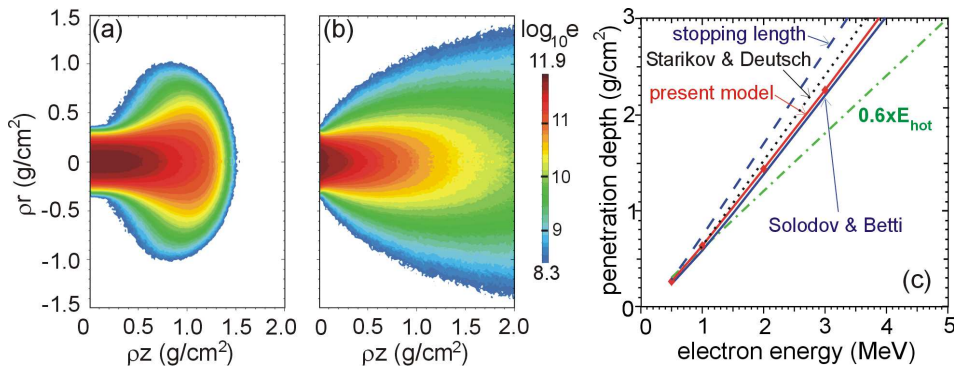


**Figure 1.** Energy deposition isocontours of (a) monoenergetic 2 MeV electrons impinging perpendicularly on a DT slab of 400 g/cm<sup>3</sup>, and (b) electrons with the spectral distribution explained in the text, mean energy  $\langle E \rangle = 2$  MeV and divergence half-angle  $\langle \theta \rangle = 22^\circ$  (HWHM). Colour isocontours are in logarithmic scale in units of J/cm<sup>3</sup>. (c) Comparison of the electron penetration depth obtained by different models.

Initial divergence angle of the relativistic electron beam is a crucial parameter for fast ignition. Recent experiments of hot electron generation and transport in solid foil targets with  $I\lambda^2$  ( $\sim 4 \times 10^{19}$  W $\mu\text{m}^2/\text{cm}^2$ ) and pulse durations  $\tau$  ( $\sim 5$  ps) relevant for fast ignition have evidenced beam divergence angles of about  $35^\circ$  [5, 6]. Our hybrid simulations can reproduce this result by assuming an initial divergence half-angle  $\langle \theta \rangle$  around  $50^\circ$ . The difference between this initial half-angle and the effective propagation full-angle of  $35^\circ$  is due to the beam collimation by self-generated azimuthal magnetic fields  $B_\theta$ , which strength increase with pulse duration as shown by equation (3). Integrated simulations for initial half-angles  $\langle \theta \rangle \geq 50^\circ$  give electron-beam ignition energies  $E_{ig} > 50$  kJ, well over the energies envisaged for the future facilities [8]. Fast electron generation in cones may reduce the beam divergence due to surface acceleration and focusing toward the cone tip [26, 27]. However, there are experimental evidences showing almost no effect of the cone on beam focusing [28]. Here, we have considered the initial beam opening half-angle as a parameter, varying from the  $22^\circ$  measured by Kodama et al. [14, 15] to the  $50^\circ$  used to reproduce the experiments mentioned above. The initial beam divergence is modelled as follows: a fast electron with kinetic energy  $E = (\gamma - 1)m_e c^2$  is randomly injected in a cone with a half-angle given by the ponderomotive scaling formula  $\theta = \tan^{-1}\{f_\theta \times [2/(\gamma - 1)]^{1/2}\}$ , where  $\gamma$  is the Lorentz factor of the electron and the parameter  $f_\theta$  is used to adjust the initial divergence half-angle of the whole electron beam. We have chosen  $f_\theta = 1$  for the reference case that corresponds to  $\langle \theta \rangle = 35^\circ$ , well below the initial divergence required to reproduce the experiments of Refs. [5, 6], but substantially higher than the  $\langle \theta \rangle = 22^\circ$  considered in previous studies [3].

Fast electron collisions with the background DT plasma are modelled by the relativistic Fokker-Planck equation with standard Coulomb cross sections. The Fokker-Planck equation is solved by the Monte Carlo method [29]. The energy deposition of a

!

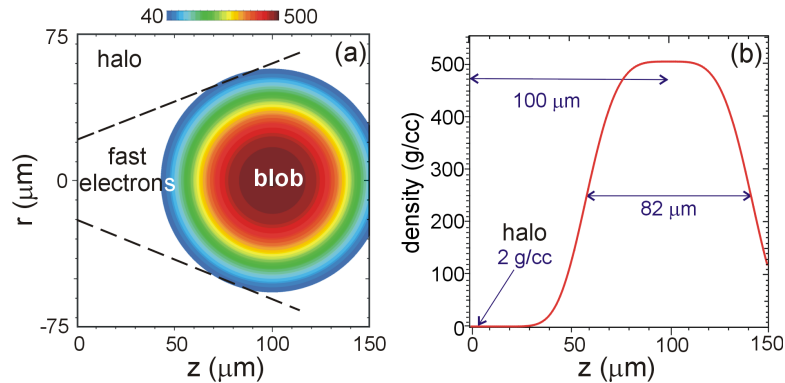


**Figure 2.** Central cut through imploded target configuration: (a) density isocontours in  $\text{g/cm}^3$  and (b) density profile at  $r = 0$ .

monoenergetic 2 MeV electron beam with a supergaussian profile in radius and a half width at half maximum (HWHM) of  $20 \mu\text{m}$  impinging perpendicularly on a  $400 \text{ g/cm}^3$  DT slab is shown in figure 1. The beam is collimated at half of its range, being subject to scattering and blooming in the second half, as reported in [30]. The fast electron penetration depth obtained with the present model is similar to that recently published by Solodov and Betti [31] and also to the quantum calculations by Starikov and Deutsch [32, 33] and about 20% larger than the scaling  $\rho R [\text{g/cm}^2] = 0.6 \times E_{\text{hot}} [\text{MeV}]$  [34], as shown in figure 1(c). It is worth noticing that the energy deposition changes significantly when beams with realistic energy and angular distributions are considered. For instance, in figure 1(b) the energy deposition is shown for the same beam as in figure 1(a), but with a mean divergence half-angle of  $22^\circ$  (within the HWHM of the super-Gaussian profile in radius) and a 1D relativistic Maxwellian distribution with mean energy  $\langle E \rangle = 2 \text{ MeV}$ . Notice the apparent range lengthening due to the beam energy spectrum and the subsequent delocalization of electron energy deposition.

Regarding the energy transport models, we have used one-group flux-limited thermal electron conduction and multigroup radiation transport. Classical Spitzer electrical and thermal conductivities are chosen for the DT plasma with the Coulomb logarithms given in Ref. [35]. Degeneracy effects have not been taken into account in the transport coefficients because the DT is heated to keV temperatures in a few ps and field generation is not important in the dense core, as will be discussed in Section 4. We have neglected also the effects of self-generated magnetic fields on transport coefficients. MPQeos tables [36] have been used to compute electron and ion temperatures from the deposited energy. Alpha-particle transport and energy deposition calculations have been performed by a 3D Monte-Carlo model with standard stopping power and mean deflection coefficients.

### 3. Imploded target configuration and beam parameters.

The target configuration used in this paper is shown in figure 2. It is a simplified version of that obtained from radiation-hydrodynamics calculations [37, 38]. It consists of 0.18 mg of DT fuel compressed into a supergaussian spherical blob with a peak density of  $500 \text{ g/cm}^3$  and  $82 \text{ }\mu\text{m}$  diameter (FWHM) placed on a density pedestal of  $2 \text{ g/cm}^3$ . The  $\rho R$  of the blob is  $2 \text{ g/cm}^2$  and the  $\rho L$  through the central cut of the simulation box is  $4 \text{ g/cm}^2$ . For simplicity, a uniform initial DT temperature of 300 eV has been assumed, which sets the initial resistivity to a level of  $3 \times 10^{-8} \text{ }\Omega\text{m}$ . We assume also that the DT is initially at rest, which is a reasonable choice because the fuel is almost stagnated at the time of peak  $\rho R$ .

A beam of fast electrons is injected from the left at  $z = 0$ . We imagine that it emerges from the tip of a cone at this position with a supergaussian profile in radius and Gaussian in time. The supergaussian profile in radius reduces the beam energy spread and enhances azimuthal magnetic field growth because from equation (3)  $\partial B_\theta / \partial t \approx \partial E_z / \partial r \approx \partial(\eta j_{b,z}) / \partial r$ . However, the lack of experimental evidences of laser-generated electron beams with such profiles makes our calculations slightly optimistic in a similar way to other fast ignition studies that assume cylindrical beams [9, 34]. More realistic calculations with a Gaussian profile have been presented in Ref. [4].

The reference case considered in this paper is defined by a distance between the cone tip and the dense blob  $d = 100 \text{ }\mu\text{m}$ , beam power of 2 PW, beam radius of  $20 \text{ }\mu\text{m}$  (HWHM), pulse duration of 18 ps at full width at half maximum (FWHM), electron mean kinetic energy within the HWHM of the radial distribution  $\langle E \rangle = 1.6 \text{ MeV}$  ( $f_T = 0.67$ ) and initial beam divergence half-angle  $\langle \theta \rangle = 35^\circ$  within the HWHM ( $f_\theta = 1$ ). The total beam energy is 36 kJ. Assuming a laser-to-fast electron conversion efficiency of 40%, this beam could be generated by a laser pulse with the same supergaussian distribution and spot radius that the electron beam, a mean intensity within the FWHM of  $2.7 \times 10^{20} \text{ W/cm}^2$ ,  $\lambda = 0.53 \text{ }\mu\text{m}$  and a total energy of 90 kJ. The second harmonic of the neodymium laser is used here to reduce the mean energy of fast electrons and maximize their coupling with the dense core. The number density of the electron beam at the injection surface is around  $2 \times 10^{22} \text{ cm}^{-3}$ , below the relativistic critical density for  $I\lambda^2 = 7.6 \times 10^{19} \text{ W}\mu\text{m}^2/\text{cm}^2$ , and a factor of  $\approx 5$  higher than the standard critical density for  $\lambda = 0.53 \text{ }\mu\text{m}$ .

Concerning the numerical parameters, we have chosen a cell width of  $1 \text{ }\mu\text{m}$  in each coordinate, a time step of 3 fs, and a total number of injected particles of  $4 \times 10^6$ . Free boundaries have been used in all simulations.

### 4. Fast electron energy deposition

We present in this Section our results on the interaction and energy deposition of the fast electron beam with the target for the reference case defined above.

In the low density halo, the beam deposits its energy mainly as Ohmic heating

!

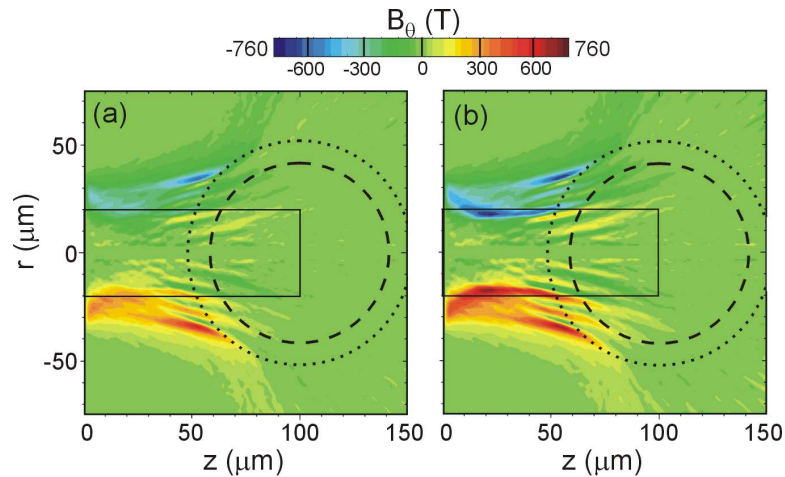


**Figure 3.** Self-generated azimuthal magnetic field  $B_\theta$  (a) at the time of peak power and (b) at the end of the pulse. The fast electron pulse has a Gaussian profile in time with a total energy of 36 kJ and a duration of 18 ps (FWHM). Beam parameters are  $d = 100 \mu\text{m}$ ,  $\langle E \rangle = 1.6 \text{ MeV}$  and  $\langle \theta \rangle = 35^\circ$ . Dashed and dotted circles show the initial position of the 250  $\text{g}/\text{cm}^3$  and 100  $\text{g}/\text{cm}^3$  isocontours, respectively. The solid line depicts the position of a perfectly collimated beam of 20  $\mu\text{m}$  radius.

by return currents. Plasma electrons are heated up to temperatures  $T_e \approx 10 \text{ keV}$  much higher than the ion temperature  $T_i$  in a few picoseconds. This temperature is almost constant while the electron beam is on because the energy transferred to plasma electrons is balanced approximately by thermal electron conduction in the direction perpendicular to the electron beam. The DT resistivity at 10 keV ( $\approx 4 \times 10^{-10} \Omega\text{m}$ ) is high enough for a GA fast electron beam to generate an azimuthal magnetic field  $B_\theta$  of hundreds of Tesla in 10 - 15 ps ( $B_\theta \approx \tau \partial E_z / \partial r \approx \tau \eta j_{b,z} / r_b = \tau \eta I_b / (\pi r_b^3)$ , where  $I_b$  stands for total current,  $r_b$  for beam radius and  $\tau$  for pulse duration). This magnetic field grows up slowly due to the low plasma resistivity and collimates the electron beam in the second half of the pulse. Azimuthal magnetic fields of a few hundreds of Tesla are sufficient to collimate most of the beam electrons. For instance, the Larmor radius of 1 MeV electron in a  $B_\theta$ -field of 250 T is around 19  $\mu\text{m}$ , similar to the 20  $\mu\text{m}$  beam radius assumed here. If thermal conduction were not taken into account, temperatures in the halo would be much higher, the  $B_\theta$ -field would saturate at levels lower than the hundreds of Tesla reported here and there would be no significant beam collimation in the halo, as it was shown in previous studies [3].

At intermediate densities  $10 < \rho < 100 \text{ g}/\text{cm}^3$ , electron temperatures are lower, resistivities higher and electron-ion energy exchange is fast enough to equilibrate electron and ion temperatures  $T_i \approx T_e$ . Higher resistivities lead to enhanced field generation and collimation of the relativistic electron beam after a few ps, as depicted in figure 3. It is worthwhile noticing that the  $B_\theta$ -field peaks in this zone and how its oscillations are attenuated towards the beam axis due to the increasing plasma density. The

!

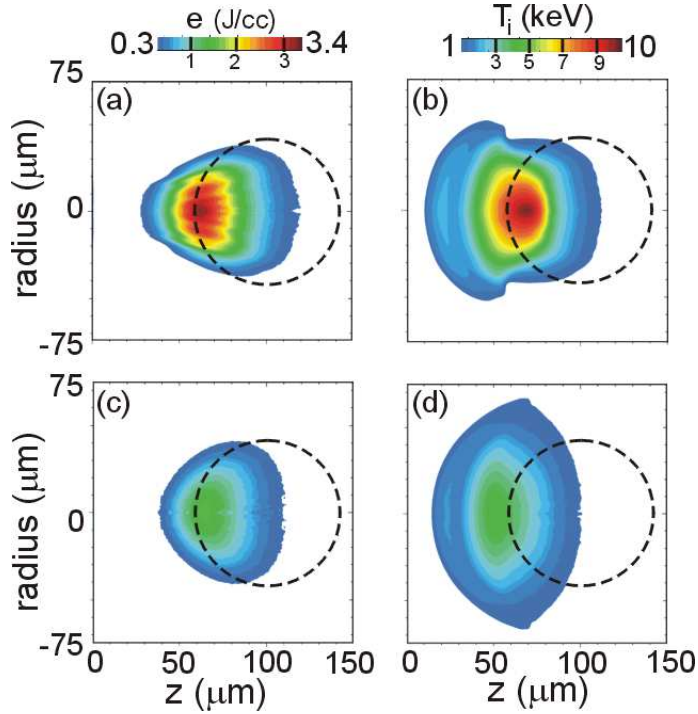


**Figure 4.** Energy density in  $\text{J}/\text{cm}^3$  deposited by the fast electron beam for the case of figure 3. Upper row [(a) and (b)]: Coulomb energy deposition and ion temperature at the end of the pulse in the full simulation with self-generated fields on. Lower row [(c) and (d)] Coulomb energy deposition and ion temperature at the end of the pulse in the simulation with self-generated fields artificially suppressed. Dashed circles show the initial position of the  $250 \text{ g}/\text{cm}^3$  density isocontour.

enhancement of the beam collimation with time can be observed by comparing the location of the peak  $B_\theta$ -field, which is near the beam edge, in Figs. 3(a) and (b).

At densities higher than  $100 \text{ g}/\text{cm}^3$ , self-generated fields are damped by collisions of beam electrons with the background plasma and DT heating is almost exclusively due to Coulomb deposition. As has been pointed out recently [3], anomalous electron stopping due to resistivity effects plays no significant role at such high densities. The overall energy balance of the reference case shows that 87% of the beam energy is deposited in the target via Coulomb collisions, 12% is carried by electrons that pass through the target and escape, 1% is deposited as Ohmic heating by return currents and around 54% is deposited at densities higher than half of the maximum ( $\rho > 250 \text{ g}/\text{cm}^3$ ). Even though only 1% of the beam energy is deposited as Ohmic heating, self-generated fields turn out to contribute to the Coulomb energy deposition in the dense core indirectly via resistive collimation of the fast electron beam, which concentrates the energy deposition in a spot slightly bigger than the initial beam diameter, as shown in figure 4(a). The effective propagation full-angle of the beam electrons near the dense core taken from Figs. 3 and 4 is, approximately,  $28^\circ$ , which gives a maximum spot diameter of  $49 \mu\text{m}$  (FWHM) at a depth of  $z = 72 \mu\text{m}$ . The energy density deposited via Coulomb collisions

!

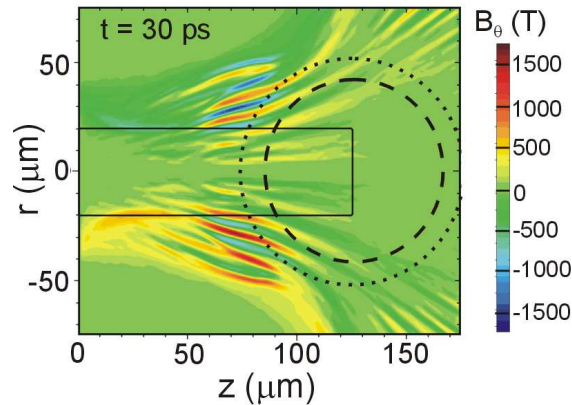


**Figure 5.** Self-generated azimuthal magnetic field  $B_\theta$  for the target pictured in figure 2 with  $d = 125 \mu\text{m}$ . The beam parameters are  $\langle E \rangle = 1.6 \text{ MeV}$ ,  $\langle \theta \rangle = 35^\circ$  and a total energy of 50 kJ. Dashed and dotted circles show the initial position of the  $250 \text{ g/cm}^3$  and  $100 \text{ g/cm}^3$  isocountours, respectively. The solid line depicts the position of a perfectly collimated beam of  $20 \mu\text{m}$  radius.

with and without self-generated fields are compared in Figs. 4(a) and (c). It is worth mentioning the enhancement of the energy density by a factor of about 2 when self-generated fields are taken into account. The oscillations shown in figure 4(a) are due to the weak filamentation of the  $B_\theta$ -field in the density ramp. These oscillations do not affect DT ignition significantly because of thermal smoothing. However, for higher distances  $d$  from cone to dense core, the beam becomes more filamented (see figure 5) and the energy deposition more fragmented than that shown in figure 4(a), imprinting the plasma density and temperature profiles.

## 5. Coupling efficiency

The electron beam coupling efficiencies (defined as the fraction of the beam energy deposited at densities higher than  $250 \text{ g/cm}^3$ ) predicted by our integrated model are depicted in figure 6(a). The corresponding electron-beam ignition energies  $E_{ig}$  are shown in figure 6(b). In all simulations we keep constant the fast electron beam intensity and increase the beam energy firstly by increasing the pulse duration up to a maximum of 20 ps and then by increasing the beam radius. For instance, the ignition energy of 57 kJ is obtained for a pulse duration of 20 ps and a beam radius of  $23.9 \mu\text{m}$  while these parameters are 18 ps and  $20 \mu\text{m}$  for the reference case of 36 kJ.

It is remarkable that, for the beam parameters chosen here, fast electrons propagate up to the top of the density ramp and deposit there a significant fraction of their energy without beam disruption or breaking-up due to the self-generated magnetic fields. Beams with lower kinetic energies are more prone to filamentation, while beams with higher kinetic energies have lower coupling efficiencies [3]. The importance of beam

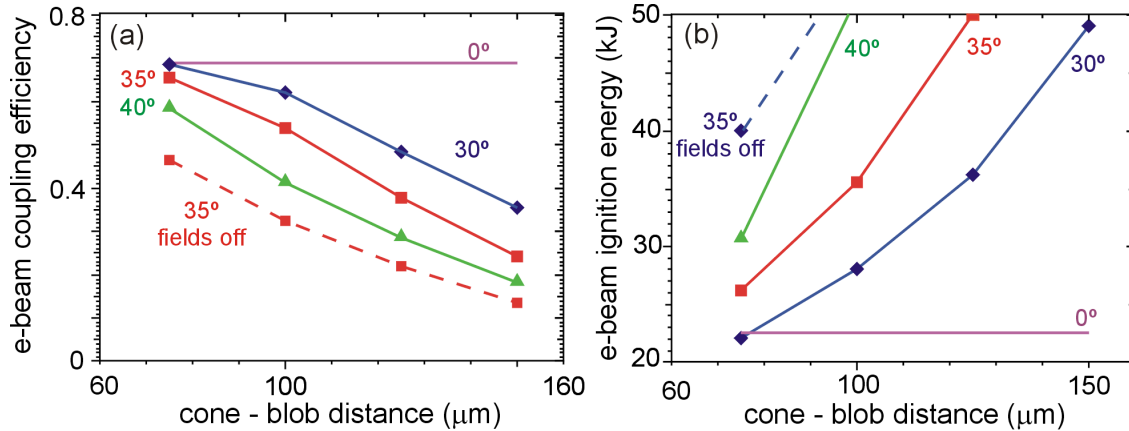


**Figure 6.** (a) Coupling efficiencies and (b) minimum ignition energies of electron beams with  $\langle E \rangle = 1.6$  MeV as function of the cone-blob distance. Curves are labelled with the initial beam divergence half-angle  $\langle\theta\rangle$ . The dashed lines and the lines labelled with  $0^\circ$  correspond to simulations with self-generated fields artificially suppressed.

collimation can be seen in figure 6(a) by comparing the coupling efficiencies for different  $d$  and  $\langle\theta\rangle$  with that obtained for a perfectly collimated beam ( $\langle\theta\rangle = 0^\circ$  and fields turned off). As shown in the figure, only for  $d = 75 \mu\text{m}$  and  $\langle\theta\rangle = 30^\circ$  the beam is nearly collimated, decreasing beam collimation with divergence angles, in agreement with the results of Bell and Kingham [39].

The dependence of the coupling efficiency on the mean kinetic energy of beam electrons is shown in figure 7. If self-generated fields are artificially suppressed, the optimal kinetic energy changes with the initial divergence half-angle from around 2 MeV for perpendicular incidence to about 1.2 MeV for  $\langle\theta\rangle = 35^\circ$ . This is due to the different target areal densities seen by fast electrons with different divergence angles. In full simulations with fields on and  $\langle\theta\rangle = 35^\circ$ , the coupling efficiencies are much higher due to beam collimation and have a maximum around 1.2 MeV, similar to that found in simulations with fields off. It is shown also in this curve the weak dependence of the coupling efficiency on mean kinetic energy for  $\langle E \rangle \leq 1.6$  MeV. For higher kinetic energies, beam current density, self-generated fields and beam collimation are lower and the coupling efficiency tends to that found with fields off.

Assuming a laser-to-fast electron conversion efficiency of 40% and a minimum overall coupling efficiency of the laser beam to the dense core of 25% [38], suitable fast ignition schemes have to have minimum electron beam coupling efficiencies around 0.6. Figure 6(a) shows that this coupling efficiency is found for  $\langle\theta\rangle \leq 35^\circ$  and distances  $d \leq 100 \mu\text{m}$ , approximately, for the target analysed here. Figure 7 adds the additional restriction that  $\langle E \rangle \leq 1.6$  MeV to achieve overall coupling efficiencies around 25%.

!

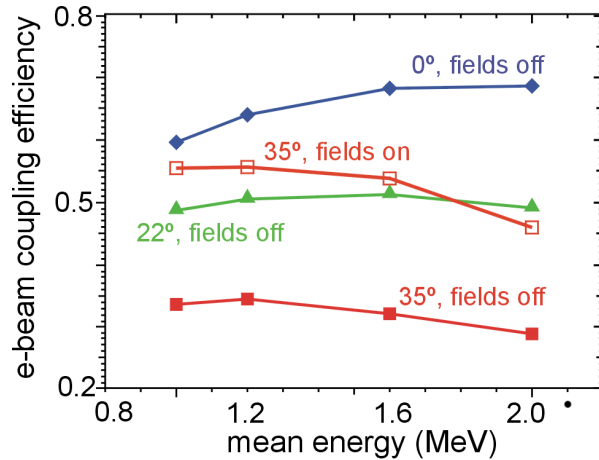


**Figure 7.** Electron beam coupling efficiency as function of the mean kinetic energy of the beam electrons. Curves with solid markers correspond to simulations with Coulomb energy deposition only. The curve with open squares corresponds to full simulations including self-generated fields. Each curve is labelled with the initial beam divergence half-angle. In all cases the distance between the cone and the blob is  $d = 100 \mu\text{m}$ .

## 6. Fuel ignition

We have performed a series of integrated simulations to obtain the ignition energies  $E_{ig}$  as a function of cone to blob distance  $d$ , initial divergence half-angle  $\langle\theta\rangle$  and mean kinetic energy of fast electrons  $\langle E\rangle$ . Typical density and ion temperature profiles near the end of the pulse and in the ignition propagation phase are depicted in figure 8, where one can see that DT expansion is not important during the beam energy deposition and becomes relevant after fusion reactions have been triggered. The ignition energies shown in this Section are obtained as the minimum beam energy for which the thermonuclear fusion power has an exponential or higher growth in time. Ignition energies as a function of  $d$  and  $\langle\theta\rangle$  for a beam with  $\langle E\rangle = 1.6 \text{ MeV}$  are plotted in figure 6(b). This figure shows the very important dependence of  $E_{ig}$  on both parameters and the crucial role played by self-generated fields. The ignition energies of figure 6(b) are 20-30% lower than those reported in previous studies [4] due to the sharper radial profile of the fast electron beam assumed here, i.e. supergaussian versus Gaussian, which concentrates the energy deposition and enhances magnetic field generation at the beam edge. Comparison of the ignition energies with that obtained for a perfectly collimated beam ( $\langle\theta\rangle = 0^\circ$  and fields turned off) shows that for  $d = 75 \mu\text{m}$  and  $\langle\theta\rangle = 30^\circ$ , the beam is almost perfectly collimated. For higher  $d$  and  $\langle\theta\rangle$ , beam collimation is still important, but the beam diverges with an angle lower than the initial divergence assumed when propagates toward the blob.

Sensitivity of the ignition energies on  $\langle\theta\rangle$  and  $\langle E\rangle$  is shown in figure 9 for a target with  $d = 100 \mu\text{m}$ . The relatively low sensitivity found for low initial divergences is a signal of beam collimation. For instance, the ignition energy  $E_{ig} = 19.5 \text{ kJ}$  obtained for

!

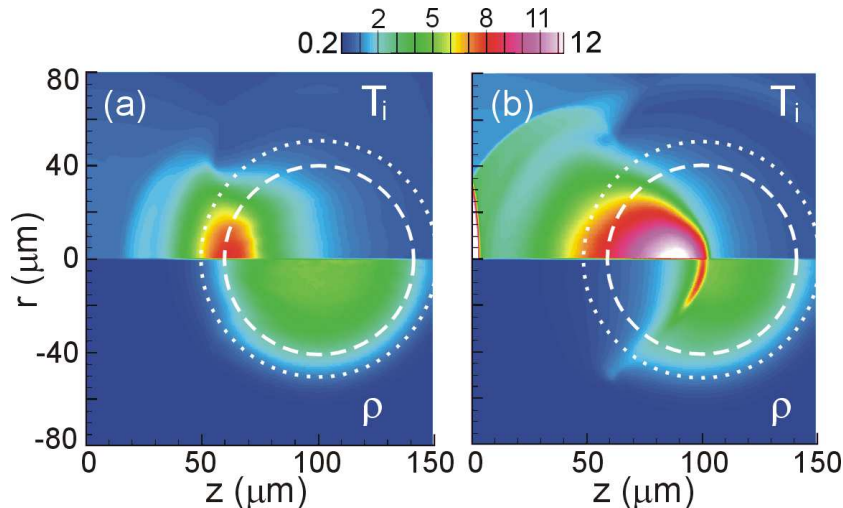


**Figure 8.** Ion temperature and plasma density isocontours for the case (a) and (b) of Figs. 4 with self-generated fields on (a) when 90% of the beam energy has been injected in the simulation box, and (b) 30 ps after the time of peak power of the fast electron beam when ignition is propagating through the DT fuel. Dashed and dotted circles show the initial position of the 250 g/cm<sup>3</sup> and 100 g/cm<sup>3</sup> density isocontours, respectively. Ion temperatures are given in keV and densities in units of 100 g/cm<sup>3</sup>.

a beam with  $\langle E \rangle = 1.6$  MeV and  $\langle \theta \rangle = 22^\circ$  is lower than that obtained for a perfectly collimated beam (22.5 kJ in figure 6(b)) due to the beam compression by the  $B_\theta$ -field. It is also worth pointing out that the lowest ignition energies are obtained for  $\langle E \rangle = 1.2$  MeV, in agreement with the coupling efficiencies shown in figure 7. However, the dependence of  $E_{ig}$  on  $\langle E \rangle$  is more pronounced than that found for the coupling efficiency due to the variation of the penetration depth with the mean kinetic energy of beam electrons.

Our integrated simulations predict that the imploded target configuration pictured in figure 2 heated by an electron beam with  $\langle E \rangle = 1.6$  MeV and  $\langle \theta \rangle = 30^\circ$  will ignite with beam energies  $E_{ig}$  between 22 and 50 kJ, depending of the distance  $d$  between the cone and the blob. For the laser-to-fast-electron conversion efficiency of 0.4 assumed, these energies correspond to laser pulses from 55 to 125 kJ, respectively. Ignition of targets with  $d = 100$   $\mu\text{m}$  by laser beam energies lower than 100 kJ requires to generate electron beams with initial divergences and mean energies within the zone defined by  $E_{ig} \leq 40$  kJ in figure 9, which sets a compromise between the beam parameters  $\langle E \rangle$  and  $\langle \theta \rangle$  for the imploded target configuration analysed here.

## 7. Conclusions

One of the main conclusions of our study is that giga-ampere, multi-PW currents can be transported through the steep gradients of the plasma corona toward the high-density fuel core and can ignite it with beam energies of 30 - 40 kJ for the electron beam

!

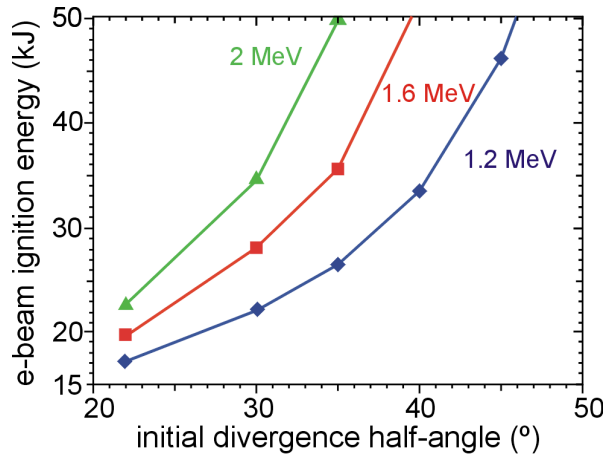


**Figure 9.** Electron beam ignition energies of the target depicted in figure 2 as a function of the initial divergence half-angle ( $\theta$ ) with the mean kinetic energy ( $\langle E \rangle$ ) as a parameter. The distance between cone and blob is  $d = 100 \mu\text{m}$  in all curves.

parameters and the target configuration assumed. The present simulations show that in the dense core, energy deposition takes place almost exclusively by classical Coulomb collisions. Self-generated fields play a major role for core heating improving the coupling efficiency substantially, but in an indirect way by means of beam collimation.

We have performed a parametric study to obtain minimum ignition energies as a function of the cone - blob distance, beam divergence and electron kinetic energy for the imploded fuel configuration considered here. We found that the ignition energy depends strongly on the cone - blob distance and the beam divergence, both crucial parameters for fast ignition. The optimal kinetic energy for the initial divergence half-angle of  $35^\circ$  is about 1.2 MeV, significantly lower than the 2 MeV found for perfectly collimated beams. Our calculations show that targets with cone - blob distances lower than  $125 \mu\text{m}$  can be ignited by electron beams with energies around 40 kJ if initial divergence half-angles are about  $30^\circ - 35^\circ$  and electron kinetic energies are lower than 1.6 MeV. Assuming a laser-to-fast electron conversion efficiency of 40%, these electron beams could be generated by the short-pulse laser beams around 100 kJ envisioned for future facilities [8]. These conclusions rely on the integrated hybrid PIC model used here, which is valid for electron transport in dense media and therefore depends on the distribution function assumed for the injected electrons. Further theoretical and experimental investigations for a full characterization of fast electron beams generated in cones by laser pulses of 10 - 20 picoseconds are necessary to estimate more precisely the energy requirements of electron-driven fast ignition.

## Acknowledgments

This work was supported by the research grants ENE2006-06339 and CAC-2007-13 of the Spanish Ministry of Education and by the Association EURATOM - IPP Garching in the framework of IFE Keep-in-Touch Activities and the Fusion Mobility Programme.

## References

- [1] Tabak M, Hammer J, Glinsky M, Kruer W L, Wilks S C, Woodworth J, Campbell E M, Perry M D and Mason R J 1994 *Phys. Plasmas* **1** 1626
- [2] Tabak M, Clark D S, Hatchett S P, Key M H, Lasinski B F, Snavely R A, Wilks S C, Town R P J, Stephens R, Campbell E M, Kodama R, Mima K, Tanaka K A Atzeni S and Freeman R 2005 *Phys. Plasmas* **12** 052708
- [3] Honrubia J J and Meyer-ter-Vehn J 2006 *Nucl. Fusion* **46** L25
- [4] Honrubia J J and Meyer-ter-Vehn J 2008 *Journal of Physics: Conference Series* **112** 022055
- [5] Green J S, Ovchinnikov V M, Evans R G, Akli K U, Azechi H, Beg F N, Bellei C, Freeman R R, Habara H, Heathcote R, Key M H, King J A, Lancaster K L, Lopes N C, Ma T, MacKinnon A J, Markey K, McPhee A, Najmudin Z, Nilson P, Onofrei R, Stephens R, Takeda K, Tanaka K A, Theobald W, Tanimoto T, Waugh J, Van Woerkom L, Woolsey N C, Zepf M, Davies J R and Norreys P A 2008 *Phys. Rev. Lett.* **100** 015003
- [6] Lancaster K L, Green J S, Hey D S, Akli K U, Davies J R, Clarke R J, Freeman R R, Habara H, Key M H, Kodama R, Krushelnick K, Murphy C D, Nakatsutsumi M, Simpson P, Stephens R, Stoeckl C, Yabuuchi T, Zepf M and Norreys P A 2007 *Phys. Rev. Lett.* **98** 125002
- [7] Chrisman B, Sentoku Y and Kemp A J 2008 *Phys. Plasmas* **15** 056309
- [8] Dunne M 2006 *Nature Phys.* **2** 2
- [9] Solodov A A, Betti R, Delettrez J A and Zhou C D 2007 *Phys. Plasmas* **14**, 062701
- [10] Bell A R, Davies J R, Guerin S and Ruhl H 1997 *Plasma Phys. Control. Fusion* **39** 653
- [11] Davies J R 2002 *Phys. Rev. E* **65** 026407
- [12] Gremillet L, Bonnaud G and Amiranoff F 2002 *Phys. Plasmas* **9** 941
- [13] Kemp A J, Sentoku Y, Sotnikov V and Wilks S C 2006 *Phys. Rev. Lett.* **97** 235001
- [14] Kodama R, Norreys P A, Mima K, Dangor A E, Evans R G, Fujita H, Kitagawa Y, Krushelnick K, Miyakoshi T, Miyanaga N, Norimatsu T, Rose S J, Shozaki T, Shigemori K, Sunahara A, Tampo M, Tanaka K A, Toyama Y, Yamanaka T and Zepf M 2001 *Nature* **412** 798
- [15] Kodama R, Shiraga H, Shigemori K, Toyama Y, Fujioka S, Azechi H, Fujita H, Habara H, Hall T, Izawa Y, Jitsuno T, Kitagawa Y, Krushelnick K M, Lancaster K L, Mima K, Nagai K, Nakai M, Nishimura H, Norimatsu T, Norreys P A, Sakabe S, Tanaka K A, Youseff A, Zepf M and Yamanaka T 2002 *Nature* **418** 933
- [16] Campbell R B, Kodama R, Mehlhorn T A, Tanaka K A and Welch D R 2005 *Phys. Rev. Lett.* **94** 055001
- [17] Mason R J 2006 *Phys. Rev. Lett.* **96** 035001
- [18] Honrubia J J, Antonicci A and Moreno D 2004 *Las. Part. Beams* **22** 129
- [19] Honrubia J J, Kaluza M, Schreiber J, Tsakiris G D and Meyer-ter-Vehn J 2005 *Phys. Plasmas* **12** 052708
- [20] Honrubia J J, Alfonsn C, Alonso L, Perez B, and Cerrada J A 2006 *Las. Part. Beams* **24** 217
- [21] Sentoku Y, Mima K, Ruhl H, Toyama Y, Kodama R and Cowan T E 2004 *Phys. Plasmas* **11** 3083
- [22] Silva L O, Fonseca R A, Tonge J W, Mori W B and Dawson J M 2002 *Phys. Plasmas* **9** 2458
- [23] Bret A, Firpo M C and Deutsch C 2005 *Phys. Rev. Lett.* **94** 115002
- [24] Pukhov A, Sheng Zh-M and Meyer-ter-Vehn J 1999 *Phys. Plasmas* **6** 2847
- [25] Nakamura T, Sentoku Y, Matsuoka T, Kondo K, Nakatsutsumi M, Norimatsu T, Shiraga H, Tanaka K A, Yabuuchi T and Kodama R 2008 *Phys. Rev. Lett.* **100** 165001

- [26] Nakamura T, Kato S, Nagatomo H and Mima K 2004 *Phys. Rev. Lett.* **93** 265002
- [27] Nakamura T, Mima K, Sakagami H and Johzaki T 2007 *Phys. Plasmas* **14** 053112
- [28] Baton S D, Koenig M, Fuchs J, Benuzzi-Mounaix A, Guillou P, Loupiau B, Vinci T, Gremillet L, Rousseaux C, Drouin M, Lefebvre E, Dorchie F, Fourment C, Santos J J, Batani D, Morace A, Redaelli R, Nakatsutsumi M, Kodama R, Nishida A, Ozaki N, Norimatsu T, Aglitskiy Y, Atzeni S and Schiavi A 2008 *Phys. Plasmas* **15** 042706
- [29] Sempau J, Fernandez-Varea J M, Acosta E and Salvat F 2003 *Nucl. Instr. Methods in Phys. Res. B* **207** 107
- [30] Li C K and Petrasso R D 2006 *Phys. Plasmas* **13** 056314
- [31] A. A. Solodov and R. Betti, *Phys. Plasmas* **15**, 042707 (2008)
- [32] Starikov K V and Deutsch C 2005 *Phys. Rev. E* **71** 026407
- [33] Deutsch C, Furukawa H, Mima K, Murakami M and Nishihara K 1996 *Phys. Rev. Lett.* **77** 2483
- [34] Atzeni S, Schiavi A and Bellei C 2007 *Phys. Plasmas* **14** 052702
- [35] Huba J D 1994 *NRL Plasma Formulary*, Naval Research Laboratory, Washington DC
- [36] Kemp A J and Meyer-ter-Vehn J 1998 *Nucl. Instr. Methods in Phys. Res. A* **415** 674
- [37] Honrubia J J, unpublished simulation of cone-targets with the code SARA-2D. See also [38].
- [38] Atzeni S, Schiavi A, Honrubia J J, Ribeyre X, Schurtz G, Nicola Ph, Olazabal-Loum M, Bellei C, Evans R G and Davies J R 2008 *Phys. Plasmas* **15** 056311
- [39] Bell A R and Kingham R J 2003 *Phys. Rev. Lett.* **91** 035003